Appl. Phys. B (2017) 123:190
DOI 10.1007/s00340-017-6763-2

Applied Physics B
Lasers and Optics

X-ray emission from a liquid curtain jet when irradiated by femtosecond laser pulses

F. Valle Brozas[1] · D. Papp[2] · L. M. Escudero[3] · L. Roso[1] · A. Peralta Conde[1]

Received: 6 February 2017 / Accepted: 1 June 2017 / Published online: 13 June 2017

Abstract Laser-based sources of ionizing radiation have attracted considerable attention in the last years for their broad potential applications. However, the stability and robustness of such sources are still issues that need to be addressed. Aiming to solve such problems, we propose a source that uses a liquid jet—rather than a solid—as a target for the production of X-rays. Liquid jets offer always a clean surface for every laser shot which represent a clear advantage over solids. In this work, we present an experimental characterization of the X-ray emission of such targets, and study the efficiency of the process when two temporally delayed pulses are used. According to the obtained results, the X-ray yield is comparable with commonly used targets.

1 Introduction

Laser-driven X-ray and electron sources have been shown lately as promising tools with applications in different scientific fields [1–9]. Based on the latest laser technology developments, nowadays is possible to generate ultrashort bunches of ionizing radiation of femtosecond/picosecond time duration with ultrahigh dose-rates 10^9 Gys^{-1}, being 1 gray (Gy) defined as the absorption of one joule of radiation energy per kilogram of matter. These values contrast with the moderate fluxes and microsecond pulses of the conventional source, e.g., X-ray tubes, so they define a new scenario for the study of the interaction between ionizing radiation and matter.

In our view, it is a particularly exciting application of such sources to high energy radiation and ultrafast radiation biology [10–13] with the aim to develop new radiotherapy strategies [14–21]. So far it is not clear the respond of living tissue over ultrahigh instantaneous radiation dosis. We may speculate that nonlinear processes become important, but the data are inconclusive being necessary further systematic research involving the broadest possible collaborations due to the multidisciplinary aspects of the problems.

In such polyhedric research, and from the point of view of the radiation generation, so far different laser-based sources have been proposed but mostly relying on solid targets, and in the direction of achieving challenging performances rather than robustness and user-friendliness (see for example [1, 2] and reference therein). For example, nowadays exist relatively simple setups capable to produce ultrashort bunches of X-rays and electrons using moderate laser intensities in the range of 10^{16}–10^{17} Wcm^{-2}. Typically, a femtosecond laser is focalized into a solid target. Thus, during the interaction, electrons are extracted by the electric field of the laser, accelerated, and reinjected into the plasma bulk once the field reverses its direction. In this process both Bremsstrahlung radiation (by the sudden loss of energy of the re-injected electrons) and the characteristic X-ray emission of the material of the target (by the creation of inner vacant in the atoms of the target) are emitted. Also, electron bunches following the reflection direction of the laser are generated. Both radiations, i.e., electrons and X-rays, inherit the temporal characteristics of the laser

✉ F. Valle Brozas
franvbv@gmail.com

[1] Centro de Láseres Pulsados, CLPU, Parque Científico, Villamayor, 37185 Salamanca, Spain

[2] ELI-ALPS,'ELI-HU Non-profit Ltd, Szeged 6720, Hungary

[3] Departamento de Biología Celular, Universidad de Sevilla and Instituto de Biomedicina de Sevilla (IBiS), Hospital, Universitario Virgen del Rocío/CSIC/Universidad de Sevilla, 41013 Seville, Spain

pulse. The resulting X-rays spectrum is a thermal distribution of around 10–20 keV.

However, and although sources based on solid targets are widely used, they present several difficulties for conducting systematic studies. When the laser interacts with the target, this results heavily damaged being necessary to move or rotate it to ensure a fresh area for the following laser shot. This limits considerably the reproducibility of the generated radiation because one can not ensure the same experimental conditions after the target movement. Also the live time, defined as the time of recording events or total time of acquisition, of the experiments is reduced by the number of laser shots that a target can handle before its replacement.

Triggered by the idea of developing robust and user-friendly sources for experiments that require extremely good statistics, we present in this manuscript the generation of laser-based soft X-rays from a liquid jet curtain (thin planar geometry) at atmospheric pressure conditions [22–26]. Avoiding vacuum results particularly important when working with biological samples and cheapens the final cost of the source. The used setup maintains a stable density profile of the liquid shot to shot, allowing a reproducible X-ray generation without the need of moving and replacing the target. Furthermore, similarly to solid target where the X-rays emission can be tuned using different materials, for liquids targets this tunability is obtained by solving different salts, for this work we have used KCl and KBr, in an adequate solvent. In the following, we will discuss the experimental setup as well as the characterization of the X-ray and electron emission. Finally, we complete our contribution with a brief summary and outlook.

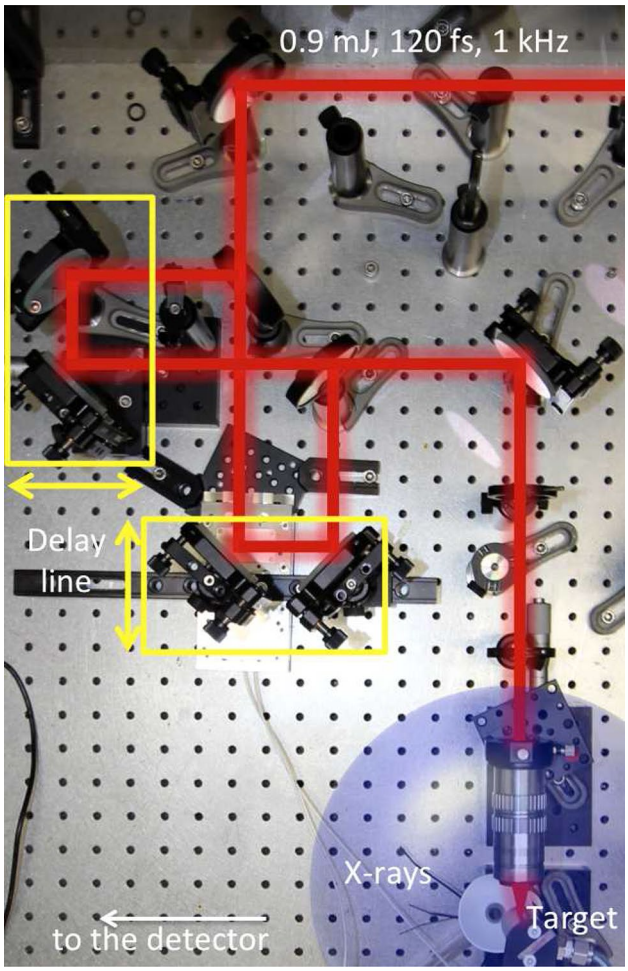

Fig. 1 Experimental setup. It is shown the configuration for the double pulses experiments

2 Experimental setup

The laser used in this work was a commercial Titanium–Sapphire femtosecond system, p-polarized, with a pulse duration of 120 fs, carrier wavelength 800 nm, repetition rate 1 kHz, and energy per pulse up to 7.5 mJ (Table 1). The spatial profile was top hat with a radius of 0.6 cm. For the generation of X-rays, just 0.65 mJ were focused into the target, i.e., into the liquid jet curtain, by a microscope objective of numerical aperture NA = 0.42 (see Fig. 1). All measurements were carried out at atmospheric pressure conditions. The achieved focal spot measured at low intensity was of the order of 1.5 μm in the horizontal and 1.2 μm in the vertical direction, being the expected intensity of the order of 10^{17} Wcm^{-2}. At the conditions for X-ray generation, i.e., using an energy per pulse of 0.65 mJ, the laser power (P ≈ 5.4 GW) exceeds the critical power for air (P_{air} ≈ 1.9 GW), being the focal spot considerably limited by laser filamentation [27]. In these conditions, we estimate a focal spot with a diameter of the order of 100 μm and a filament extension of around 200 μm-measured by imaging the plasma created by filamentation in air-yielding to an intensity of the order of 10^{14} Wcm^{-2}. The relative position between the focal spot and the liquid target was optimized by maximizing the X-ray production yield. It is noticeable that even at such low intensities X-ray and electron bunches are produced. The angle of incidence into the target was 45°. The X-ray production was detected by an Amptek Silicon drift detector (SDD-132). All experiments took place in a laboratory provided with nuclear safety measures in agreement with the Spanish Nuclear Security Council. The critical optical elements, e.g., the target holder, were controlled remotely.

The liquid jet curtain used as target was generated by a dye circulator connected to a nozzle (Sirah lasertechnik). This kind of circulators are normally used to provide the active medium for CW lasers. However for X-ray production we used rather than the solution of a laser dye in a organic

Table 1 Main laser parameters

Wavelength	800 nm	Energy per pulse	0.65 mJ
Pulse duration	120 fs	Spatial profile	Top hat $r = 0.6$ cm
Repetition rate	1 kHz	Achieved intensity	$10^{14}\,\mathrm{Wcm^{-2}} < \mathrm{I} < 10^{17}\,\mathrm{Wcm^{-2}}$

solvent, e.g., ethylene glycol, a mixture of water, glycerin and potassium chloride (KCl) or potassium bromide (KBr). In principle, and according to specifications, it is possible to use different salts with different concentrations, always that the solution has a density similar to ethylene glycol (1.1132 g/cm^3). Otherwise the liquid jet become unstable and the nozzle can get damage. We achieved that with a mixture of 65% of glycerol and 35% of water in weight. Although the solubility of KCl in water is 34.2 g/100 g, we used just 25 g/100 g for precaution. For KBr we just used 28.6 g/100 g being the solubility in water 67.8 g/100 g. Neither the solvents, i.e., water or glycerol, nor the solute present a significant absorption for 800 nm radiation. However, the density of the plasma generated at the first stages of the laser–target interaction ($n \sim 10^{21}-10^{22}\,\mathrm{cm^{-3}}$) was of the order of the critical density for 800 nm radiation ($n_c \sim 10^{21}\,\mathrm{cm^{-3}}$), being therefore most of the laser pulse reflected by this plasma. The circulator was operating at a stagnation pressure of 7 bars although it is possible to obtain a stable jet without flickering and/or air bubbles for a wide range of pressures. The dimensions of the jet were ~65 μm thickness times 4 mm in the widest part (see Fig. 2).

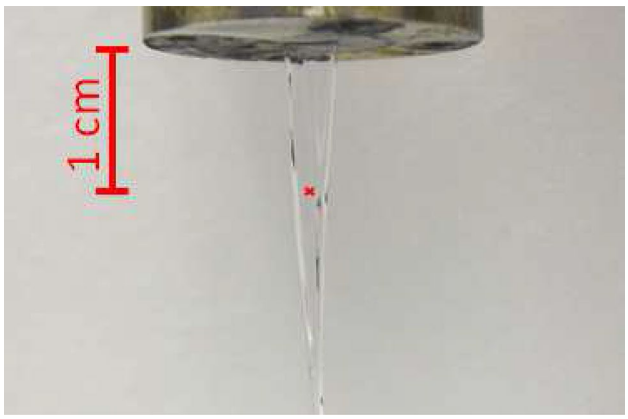

Fig. 2 Liquid jet. Dimensions: 4 mm wide × ~65 μm thick. The laser is shot at 1 cm of the jet as the cross indicates

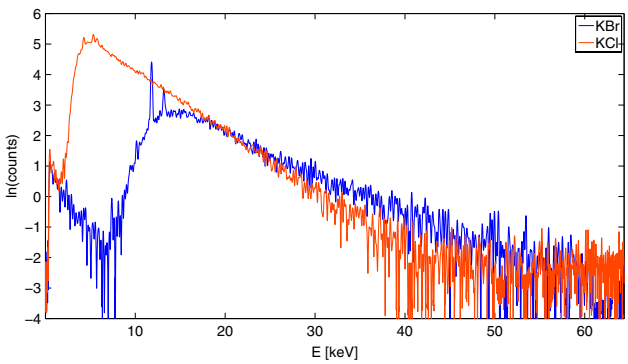

Fig. 3 (Color online) Typical X-ray spectrum for a solution of KBr or KCl

3 Source characterization

Figure 3 shows a typical X-ray spectrum for a solution of glycerin, water and KBr, and glycerin, water and KCl. For all spectra showed in this work we have applied a Fourier Transform Filter (FFT) to avoid the fast oscillations produced by spurious noise. Both spectra are defined by a Bremsstrahlung emission extending to approximately 60 keV produced in the bulk of the liquid jet, and the characteristic X-ray emission of the solute. Concretely, we can see the K_α and K_β lines of Br at 11.9 and 13.3 keV. The X-ray emission of Cl and K couldn't be detected (K_α = 2.6 keV and K_β = 2.8 keV for Cl, and K_α =3.3 keV and K_β = 3.6 keV for K) because it is absorbed by air and filters [28]. The differences in the spectra for the low energy emission are due to a 1 cm methacrylate filter used for recording the spectrum of KBr.

To obtain the efficiency of the liquid target, we can compare the K_α energy conversion for KBr and for solid Cu targets which have been routinely used so far [8, 9]. Figure 4 shows the spectra used for this comparison. Both measurements were taken in the same conditions: we placed the detector in the laser reflexion direction at a distance of 55 cm from the target. We filtered the radiation with a 1 cm thickness methacrylate filter to avoid pile up. The mass attenuation coefficient of methacrylate and air can be found in [28].

According to Fig. 4, we registered 0.0009 counts per laser pulse for the K_α line of Cu at 8.0 keV, and 0.011 counts per laser pulse for the K_α line of Br at 11.9 keV. To calculate correctly the efficiency of the source, it is necessary to take into account all the elements that reduce the X-ray photon flux prior reaching the detector: 54 cm path in air and 1 cm thickness methacrylate filter. Also, we must consider the efficiency of the detector given by the manufacturer, which has also into account the absorption in the beryllium window of the device. If we assume a 4π distribution for the K_α emission, the number of

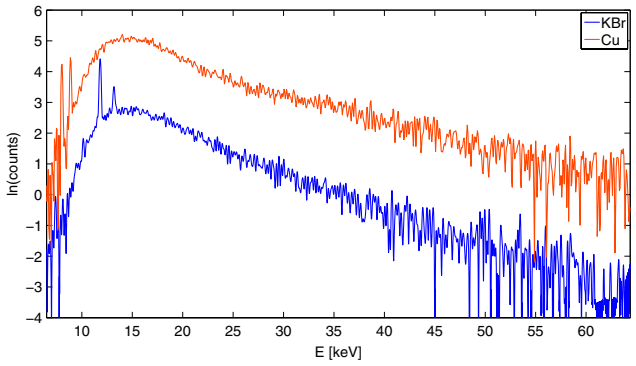

Fig. 4 (Color online) Spectra comparison between the emission of a liquid target jet—solution of KBr—and a solid Cu target

K_α photons emitted by the source per laser pulse can be written as:

$$N_{photons} = \frac{N_{counts}}{t_{acq.} RR} \frac{1}{T_{filters} \epsilon} \frac{4\pi r^2}{A} \quad (1)$$

where $t_{acq.}$ is the total acquisition time (around 300 s), RR the laser repetition rate (1 kHz), $T_{filters}$ the transmission of air and methacrylate, ϵ the efficiency of the detector for the selected K_α line, r is the distance to the detector (55 cm), and A the effective area of the detector (25 mm^2). Introducing all these data in Eq. 1, we obtain finally 7.79×10^4 photons per pulse for Cu K_α line, and 1.16×10^4 photons per pulse for Br K_α line. The efficiency μ in the K_α production is

$$\mu = N_{photons} \frac{E_{K_\alpha}}{E_{laser}} \quad (2)$$

where E_{laser} is the energy of the laser pulse. In result, we obtain a efficiency of 1.5×10^{-7} for solid Cu, and 3.4×10^{-8} for the liquid solution of KBr.

In literature one can find several works reporting the efficiency of different targets in vacuum conditions. For example, for Cu targets (wire and tape) the efficiency range from 10^{-7} to 10^{-5} [29–32], while for molybdenum (Mo) disks one can obtain slightly higher efficiencies of the order of 10^{-5} [5, 7]. The efficiency of liquid sources in vacuum has been also subject of research. Tompkins et al. measured an efficiency of 10^{-8} for 200 μm water jet with solved copper (II) nitrate [$Cu(NO_3)_2$] [25], while for a gallium (Ga) jet Zhavoronkov et al. measured an efficiency of 10^{-6} [24]. The efficiency reported in this work for liquid target jets at atmospheric pressure conditions is smaller (10^{-8}) than those values. We attribute these differences to the absorption of air and the limitation imposed by filamentation for the minimum achievable focal spot. This leads to a lower intensity and, thus, a lower electron temperature. In spite of this difference, the advantage of working at much simpler experimental conditions and with a target that does not need replacement, compensate by far this yield reduction. This information is summarized in Table 2.

Aiming to fully characterize the liquid curtain jet source, Fig. 5 shows the X-ray yield for KBr solution as a function of the laser pulse energy. Interestingly, although the emission yield decreases with the energy, even for low energies there is an appreciable X-ray generation. Below 0.1 mJ the X-ray emission was so weak that couldn't be detected by our detector. For a better understanding of Figs. 5 and 6 shows the integrated K_α peaks as a function of the laser energy.

Another interesting aspect to study is the directionality of the X-ray emission which can not be properly measured for solid targets. Figure 7 shows the X-ray spectrum for different angles of emission resulting completely isotropic. The slightly smaller yield production for the rear direction, i.e., in the direction of the laser incidence, is produced by the absorption of the formed plasma. It is interesting to mention that although the K_α and K_β emission are expected to be isotropic, for the Bremsstrahlung this is not so clear. The nature of the Bremsstrahlung

Table 2 Summary of the efficiencies for different targets

Target	Vacuum conditions	Efficiency	References
Cu (wire and tape)	Yes	10^{-7} to 10^{-5}	[29–32]
Mo disks	Yes	10^{-5}	[5, 7]
Water jet with $Cu(NO_3)_2$	Yes	10^{-8}	[25]
Ga jet	Yes	10^{-6}	[24]
Cu	No	10^{-7}	This work
KBr solution	No	10^{-8}	This work

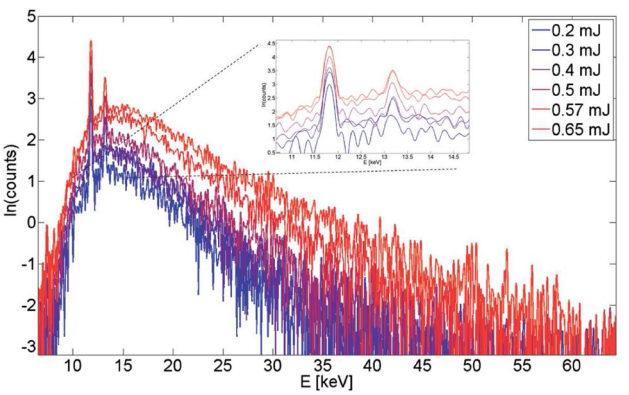

Fig. 5 X-ray spectrum for a KBr solution liquid target as a function of the pulse energy

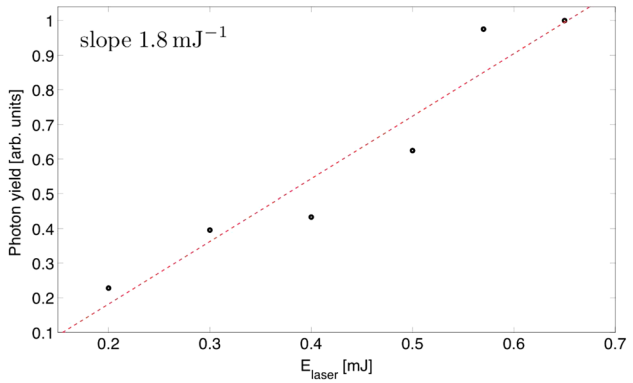

Fig. 6 Integrated K_α peaks as a function of the laser energy

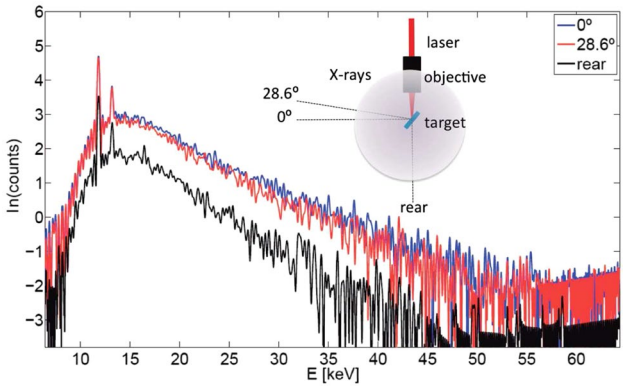

Fig. 7 X-ray spectrum for a KBr solution liquid target as a function of the emission angle

emission—this is produced by the sudden loss of energy of accelerated electrons reinjected in the plasma bulk—and the fact that, as we will show later, the accelerated electrons are produced exclusively in the reflection direction of the laser radiation may introduce some sort of anisotropy in the emission. In fact for conventional X-ray tubes, this anisotropy is well established depending on the energy of the accelerated electrons [33]. While for electrons with few keV the emission is quasi-isotropic, for higher energies the emission is predominant in the forward direction.

For laser-based sources, It is known that the distribution of laser accelerated electrons can be described by two Maxwell distributions, corresponding to the electrons that are accelerated directly by the laser (hot electrons), and those accelerated in the plasma expansion (cold electrons) [34]. The Bremsstrahlung produced by a Maxwell distribution of electrons is described by [34]

$$\frac{dN_\gamma}{dE_\gamma} \propto \frac{2e^{\frac{-E_\gamma}{kT_e}}\sqrt{E_\gamma kT_e} + (kT_e - 2bE_\gamma)\sqrt{\pi}\,\mathrm{erfc}\left(\sqrt{\frac{E_\gamma}{kT_e}}\right)}{3E_\gamma kT_e\sqrt{\pi}}. \quad (3)$$

For $T_e < E_\gamma$ we can approximate this expression by:

$$\frac{dN_\gamma}{dE_\gamma} \propto \frac{2e^{\frac{-E_\gamma}{kT_e}}}{3\sqrt{\pi E_\gamma kT_e}}. \quad (4)$$

If we correct those spectra for KBr showed in Fig. 7 for the X-ray absorption of air and methacrylate, and for efficiency of the detector, we can obtain the hot electron temperature T_{hot} fitting the most energetic part of the spectrum (see Fig. 8). The obtained temperature $T_{hot} = 24.2\,keV$ is in agreement with an isotropic Bremsstrahlung distribution [33]. For T_{cold}, the Bremsstrahlung generated by the cold electrons and the K_α and K_β emission are superimposed. Thus, it is not possible to obtain a reliable fitting of the data.

According to the obtained T_{hot}, we can discard Brunel absorption as the main laser–plasma interaction mechanism [35]. In this case, the energy of the expelled electrons is described by [36],

$$T_{hot} = 8\left(\frac{I}{10^{16}}\lambda^2\right)^{1/3}\ [keV] \quad (5)$$

where I is the laser intensity in Wcm^{-2} and λ the laser wavelength in μm. A $T_{hot} = 24.2\,keV$ corresponds to an intensity of the order of $10^{17}\,Wcm^{-2}$ which is beyond the capabilities of our experimental setup at atmospheric pressure conditions due to the limitation in the focal spot size imposed by filamentation. For the resonance absorption mechanism the energy of the expelled electrons is slightly higher [37]

$$T_{hot} \approx 14\left(\frac{I}{10^{16}}\lambda^2\right)^{1/3} T_{cold}^{1/3}\ [keV]. \quad (6)$$

Assuming a cold electron temperature of $T_{cold} = 10\,keV$, the required intensity is in the order of $10^{15}\,Wcm^{-2}$, which corresponds to a focus diameter of ~30 μm. This

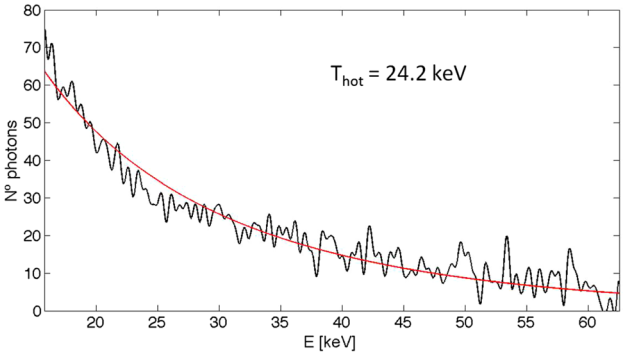

Fig. 8 High energy X-ray spectrum for KBr fitted by Eq. 4

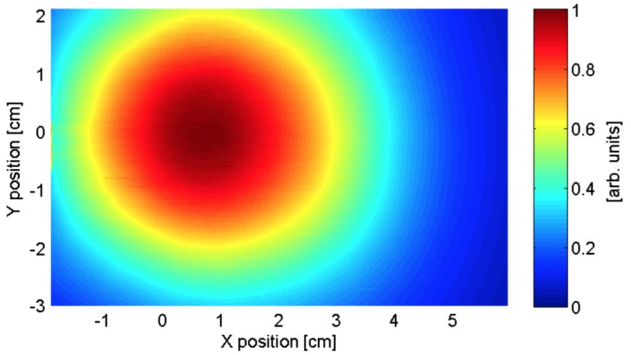

Fig. 9 Dose profile in arbitrary units registered in a gafchromic film for liquid KBr target

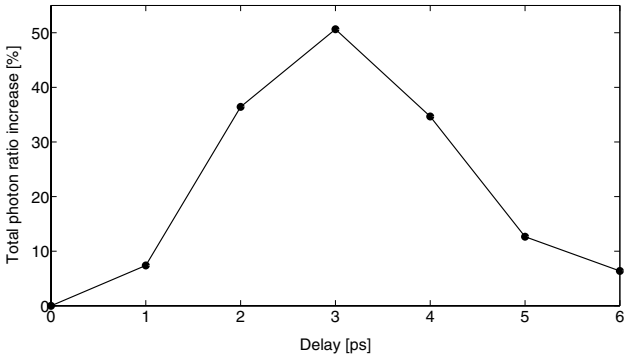

Fig. 10 Increase in X-ray yield as a function of the delay between the pulses

value is in between the measured diameter for low energies 1 μm and the limitation imposed by filamentation in air 100 μm. This difference can be understood if we take into account that once the plasma is formed, i.e., just after the interaction of the early stages of the laser pulse with the target, the filamentation process takes place in a medium with a different diffraction index than air allowing a slightly tighter focusing. It is important to remark that so far we have only hints about the relevant acceleration mechanisms. For a reliable description, it is mandatory to run complex PIC (particle-in-cell) simulations of the interaction of a filamenting femtosecond laser with a target.

Figure 9 shows the electron emission direction. These measurements were carried out placing a EBT2 gafchromic film at 5 cm from the target in the laser reflection direction. The exposition time was short enough to ensure that signature in the film was exclusively produced by the accelerated electrons. As expected, the electron emission is directional corresponding the position ($x = 0$, $y = 0$) to laser reflection direction.

4 X-ray emission by double pulses

The influence of a prepulse in laser-based X-ray generation has been proved in several experiments (see for example [38–42, 44–46]). The observed enhancement is related with the increased coupling of the stronger second laser pulse with an expanding plasma—created by the first weaker pulse—from the target surface. This expansion takes place in the picosecond time scale, and leads to a volume increase producing a smoother density profile, and, hence, a reduction in the opacity of the plasma. Since the laser-X-ray conversion efficiency strongly depends of the density gradient of the expanding plasma, at a certain delay the laser–plasma coupling is maximized. If the delay between the laser pulses is too small the density profile is still steep and there is not any difference in the laser–plasma coupling. On the other hand, if the delay is too large, the density drops rapidly and the second laser cannot efficiently heat the plasma electrons with the subsequent reduction in the X-ray emission.

To study this phenomenon we slightly modified the setup described above. The original laser radiation was divided using a beam splitter 20:80 into a prepulse and a main pulse (see Fig. 1). The delay between both pulses was controlled with a precision motorized delay stage with submicron precision. Once delayed one pulse with respect to the other, they were set collinear by a beam combiner, and focalized by the microscope objetive into the same spot (see Fig. 1). The final energy of the pulses were approximately 0.24 and 0.10 mJ. The different spectra were taken during 5 min, at a distance of 55 cm, in the direction of laser reflection. The radiation was filtered by 1 cm of methacrylate to avoid pile up. For each delay we recorded the spectrum generated by both pulses independently, and by the combined effect of them. At this low energy, the prepulse laser did not produce any measurable X-ray emission. Figure 10 shows the X-ray yield increase with respect to the situation when both pulses are temporally overlapping. We can clearly see for a delay of ∼3 ps an increment in the X-ray yield up to 50%. This result is compatible with the enhancement observed by Hatanaka et al. [42] although there are certain differences in the experimental setup. The pulses used in this work are considerable shorter, 120 fs versus 260 fs, and the laser was set parallel for both pulses (p-polarized) while in [42] the prepulse is s-polarized and the main pulse p-polarized.

5 Conclusions

In this work we have shown the potential of liquid jets as a target for X-ray production in air, characterizing their main properties experimentally. Although the X-ray emission

efficiencies for liquid and solid targets are comparable, the main advantages of liquids are their robustness and stability. Since there is no need to replace or move the target to ensure a fresh zone for every laser shot, as it is the case for solids, it is possible to carry out systematic and/or long-live measurements. These characteristics are mandatory if we want to explore the challenging possibilities that laser-based sources of ionizing radiation offer.

In a near future, we hope to investigate the possibilities of this laser-based source of ionizing radiation as a new tool for radiotherapy treatments. We will compare this source with a conventional continuous one, e.g., an X-ray tube, using the Drosophila Melanogaster—concretely the imaginal disc tissue—as animal model. For such studies, since no tissue penetration is required, few keV radiation is sufficient to induce a biological response of the tumoral tissue after irradiation. Furthermore, bearing in mind that most of the DNA damage in radiotherapy treatments is induced by radicals—oxidative and reductive DNA damage—generated by water radiolysis and this process peaks around 10 eV, maybe it is a good strategy to further reduce the energy of the radiation. With these studies we want to shed some light on two main questions: can ultrabright instantaneous fluxes of ionizing radiation trigger non-linear phenomena in the cellular medium with therapeutic effects? Can we get some inside in the ultrafast dynamics of the interaction between the tumoral tissue and the ionizing radiation? These questions are just the entrance door to a vast and unexplored field of research with challenging possibilities.

Acknowledgements The authors thank J.M. Álvarez and S. Malko for fruitful and stimulating discussions during the development of this manuscript. This work has been possible by the support from Ministerio de Educación Cultura y Deporte (F. Valle Brozas studentship FPU AP2012-3451) and Ministerio de Economía y Competitividad of Spain (FURIAM project FIS2013-47741-R, PALMA project FIS2016-81056-R).

References

1. H. Daido, M. Nishiuchi, A.S. Pirozhkov, Prog. Rep. Phys. **75**, 056401 (2012)
2. A. Macchi, M. Borghesi, M. Passoni, Rev. Mod. Phys. **85**, 751 (2013)
3. B.B. Zhang, S.S. Sun, D.R. Sun, Y. Tao, Rev. Sci. Instrum. **85**, 096110 (2014)
4. K.A. Ivanov, D.S. Uryupina, R.V. Volkov, A.P. Shkurinov, I.A. Ozheredov, A.A. Paskhalov, N.V. Eremin, A.B. Saveléva, Nuc. Inst. Meth. Phys. Res. A **653**, 5861 (2011)
5. B. Hou, J. Nees, A. Mordovanakis, M. Wilcox, G. Mourou, L.M. Chen, J.-C. Kieffer, C.C. Chamberlain, A. Krol, Appl. Phys. B **83**(1), 81–85 (2006)
6. H. Witte, M. Silies, T. Haarlammert, J. Hüve, J. Kutzner, H. Zacharias, Appl. Phys. B **90**, 11–14 (2008)
7. M. Li, K. Huang, L. Chen, W. Yan, M. Tao, J. Zhao, Y. Ma, Y. Li, J. Zhang, Radiat. Phys. Chem. (2016)
8. F. Valle Brozas, A.V. Carpentier, C. Salgado, J.I. Apinaniz, M. Rico, M.Sánchez Albaneda, J.M. Álvarez, A. Peralta Conde, L. Roso, Rev. Esp. Fis. **29**(3), 17–21 (2015)
9. F. Valle Brozas, A. Crego, L. Roso, A. Peralta Conde, Appl. Phys. B **122**, 220 (2016)
10. V. Malka, J. Faure, Y.A. Gauduel, Rev. Mutat. Res. **704**(13), 142151 (2010)
11. Y. Gauduel, S. Fritzler, A. Hallou, Y. Glinec, V. Malka, SPIE **5463**, 86–96 (2004)
12. V. Malka, J. Faure, Y. Gauduel, E. Lefebvre, A. Rousse, K.T. Phuoc, Nat. Phys. **4**, 447453 (2008)
13. A. Giulietti, M.G. Andreassi, C. Greco, SPIE Proceedings 80791J, (2011)
14. R. Meesat, H. Belmouaddine, J.F. Allard, C. Tanguay-Renaud, R. Lemay, T. Brastaviceanu, L. Tremblay, B. Paquette, J.R. Wagner, J.-P. Jay-Gerin, M. Lepage, M.A. Huels, D. Houdea, Proc. Natl. Acad. Sci. USA **109**, 38 (2012)
15. O. Rigaud, N.O. Fortunel, P. Vaigot, E. Cadio, M.T. Martin, O. Lundh, J. Faure, C. Rechatin, V. Malka, Y.A. Gauduel, Cell Death Dis. **1**, e73 (2010)
16. C. Tillman, G. Grafstrom, A.C. Jonsson, B.A. Jonsson, I. Mercer, S. Mattsson, S.E. Strand, S. Svanberg, Radiology **213**, 860–865 (1999)
17. K. Zeil, M. Baumann, E. Beyreuther, T. Burris-Mog, T.E. Cowan, W. Enghardt, L. Karsch, S.D. Kraft, L. Laschinsky, J. Metzkes, D. Naumburger, M. Oppelt, C. Richter, R. Sauerbrey, M. Schürer, U. Schramm, J. Pawelke, Appl. Phys. B **110**, 4 (2013)
18. S.D. Kraft, C. Richter, K. Zeil, M. Baumann, E. Beyreuther, S. Bock, M. Bussmann, T.E. Cowan, Y. Dammene, W. Enghardt, U. Heibig, L. Karsch, T. Kluge, L. Laschinsky, E. Lessmann, J. Metzkes, D. Naumburger, R. Sauerbrey, M. Schurer, M. Sobiella, J. Woithe, U. Schramm, J. Pawelke, New J. Phys. **12**, 085003 (2010)
19. J. Nguyen, Y. Ma, T. Luo, R.G. Bristow, D.A. Jaffray, Q.-B. Lu, Proc. Natl. Acad. Sci. USA **108**, 11778 (2011)
20. X. Kong, S.K. Mohanty, J. Stephens, J.T. Heale, V. Gomez-Godinez, L.Z. Shi, J.S. Kim, K. Yokomori, M.W. Berns, Nucleic Acids Res **37**, 9 (2009)
21. A. Yogo, T. Maeda, T. Hori, H. Sakaki, K. Ogura, M. Nishiuchi, A. Sagisaka, H. Kiriyama, H. Okada, S. Kanazawa, T. Shimomura, Y. Nakai, M. Tanoue, F. Sasao, P.R. Bolton, M. Murakami, T. Nomura, S. Kawanishi, K. Kondo, Appl. Phys. Lett. **98**, 053701 (2011)
22. L. Miaja-Avila, G.C. OŃeil, J. Uhlig, C.L. Cromer, M.L. Dowell, R. Jimenez, A.S. Hoover, K.L. Silverman, J.N. Ullom, Struct. Dyn. **2**, 024301 (2015)
23. G. Korn, A. Thoss, H. Stiel, U. Vogt, M. Richardson, T. Elsaesser, M. Faubel, Opt. Lett. **27**, 866 (2002)
24. N. Zhavoronkov, Y. Gritsai, G. Korn, T. Elsaesser, Appl. Phys. B **79**, 663–667 (2004)
25. R.J. Tompkins, I.P. Mercer, M. Fettweis, C.J. Barnett, D.R. Klug, L.G. Porter, I. Clark, S. Jackson, P. Matousek, A.W. Parker, M. Towrie, Rev. Sci. Instrum. **69**, 3113 (1998)
26. D. Papp, R. Polanek, Z. Lecz, L. Volpe, A. Peralta Conde, A.A. Andreev, IEEE Trans. Plasma Sci. **44**, 10 (2016)
27. S.L. Chin, S.A. Hosseini, W. Liu, Q. Luo, F. Théberge, N. Aközbek, A. Becker, V.P. Kandidov, O.G. Kosareva, H. Schroeder, Can. J. Phys. **83**, 863–905 (2005)
28. NIST. X-ray Mass attenuation coefficients. https://www.nist.gov/pml/x-ray-mass-attenuation-coefficients. Accessed 11 Apr 2017
29. N. Zhavoronkov, Y. Gritsai, M. Bargheer, M. Woerner, T. Elsaesser, Appl. Phys. Lett. **86**, 244107 (2005)
30. Y. Jiang, T. Lee, C.G. Rose-Petruck, J. Opt. Soc. Am. B **20**, 229237 (2003)

31. T. Guo, C. Rose-Petruck, R. Jimenez, F. Raksi, J.A. Squier, B.C. Walker, K.R. Wilsom, C.P.J. Barty, SPIE **3157**, 84 (1997)
32. Y. Jiang, T. Lee, W. Li, G. Ketwaroo, G. Rose-Petruck, Opt. Lett. **27**, 963 (2002)
33. F.M. Khan, *The physics of radiation therapy* (Lippicott Williams & Wilkins, Philadelphia, 2003)
34. P. Gibbon, *Short pulse laser interaction with matter* (Imperial College Press, London, 2007)
35. F. Brunel, Phys. Rev. Lett. **59**, 52 (1987)
36. A.A. Andreev, J. Limpouch, A.N. Semakhin, Bull. Russ. Acad. Sci. **58**, 10561063 (1994)
37. D.W. Forslund, J.M. Kindel, K. Lee, Phys. Rev. Lett. **39**, 284288 (1977)
38. J.F. Pelletier, M. Chaker, J.C. Kieffer, J. Appl. Phys. **81**, 5980 (1997)
39. R. Lokasani, G. Arai, Y. Kondo, H. Hara, T.-H. Dinh, T. Ejima, T. Hatano, W. Jiang, T. Makimura, B. Li, P. Dunne, G. O'Sullivan, T. Higashiguchi, J. Limpouch, Appl. Phys. Lett. **109**, 19 (2016)
40. R. Fazeli, M.H. Mahdieh, Phys. Plasmas **22**, 11 (2015)
41. A. Andreev, J. Limpouch, A.B. Iskakov, H. Nakano, Phys. Rev. E **65**, 026403 (2002)
42. K. Hatanaka, H. Ono, H. Fukumura, Appl. Phys. Lett. **93**, 0641013 (2008)
43. P. Zhu, Z. Zhang, L. Chen, J. Zheng, R. Li, W. Wang, J. Li, X. Wang, J. Cao, D. Qian, Z. Sheng, J. Zhang, Appl. Phys. Lett. **97**, 211501 (2010)
44. U. Teubner, G. Kühnle, F.P. Schäfer, Appl. Phys. B **54**, 493 (1992)
45. J.R. Freeman, S.S. Harilal, A. Hassanein, J. Appl. Phys. **110**, 083303 (2011)
46. S. Fujioka, M. Shimomura, Y. Shimada, S. Maeda, H. Sakaguchi, Y. Nakai, T. Aota, H. Nishimura, N. Ozaki, A. Sunahara, K. Nishihara, N. Miyanaga, Y. Izawa, K. Mima, Appl. Phys. Lett. **92**, 241502 (2008)